

Warm-starting active-set solvers using graph neural networks

Ella J. Schmidtbreick

ELLA-JOHANNA.SCHMIDTOBREICK@IT.UU.SE

Daniel Arnström

DANIEL.ARNSTROM@IT.UU.SE

Paul Häusner

PAUL.HAUSNER@IT.UU.SE

Jens Sjölund

JENS.SJOLUND@IT.UU.SE

Department of Information Technology, Uppsala University, Sweden

Abstract

Quadratic programming (QP) solvers are widely used in real-time control and optimization, but their computational cost often limits applicability in time-critical settings. We propose a learning-to-optimize approach using graph neural networks (GNNs) to predict active sets in the dual active-set solver `DAQP`. The method exploits the structural properties of QPs by representing them as bipartite graphs and learning to identify the optimal active set for efficiently warm-starting the solver. Across varying problem sizes, the GNN consistently reduces the number of solver iterations compared to cold-starting, while performance is comparable to a multilayer perceptron (MLP) baseline. Furthermore, a GNN trained on varying problem sizes generalizes effectively to unseen dimensions, demonstrating flexibility and scalability. These results highlight the potential of structure-aware learning to accelerate optimization in real-time applications such as model predictive control.

1. Introduction

Optimization problems with quadratic objectives and linear constraints, referred to as quadratic programs (QPs), form the foundation of numerous applications, including robotics (Kuindersma et al., 2014), control (Bartlett et al., 2002), and finance (Gondzio and Grothey, 2007; Mitra et al., 2007). Given their prevalence, efficient and reliable solution methods are critical for practical applications.

Convex QPs can be solved to global optimality using numerical optimization methods with polynomial complexity (Nocedal and Wright, 1999). While interior point methods are highly effective in general, their inability to leverage approximate solutions from related instances reduces their efficiency for sequences of related problems. In contrast, active-set methods naturally accommodate this technique, known as warm starting, by iteratively refining a hypothesis of the active constraint set, making them particularly well suited for small- and medium-scale problems and for detecting infeasibility (Nocedal and Wright, 1999).

Solving QPs efficiently is critical in real-time model predictive control (MPC) applications (Borrelli et al., 2017). These applications provide sequences of closely related optimization problems, making it ideal to exploit solutions from previous iterations. However, naively using the previous solution as a starting iterate can exacerbate worst-case solution time (Herceg et al., 2015). Recent works have explored ways of finding warm starts by using machine learning to adapt optimization solvers to problem classes characterized by prior instances (Chen et al., 2022b; Amos, 2023).

These learning-to-optimize approaches vary in how closely they adhere to conventional solvers. Some focus on tuning hyperparameters (Sambharya and Stellato, 2024; Doerks et al., 2025), others learn entire update steps as a black box (Andrychowicz et al., 2016), and hybrid methods combine learned updates with traditional steps to retain convergence guarantees (Banert et al., 2024). Sambharya et al. (2023) employs a end-to-end approach by predicting the points to warm-start the solver,

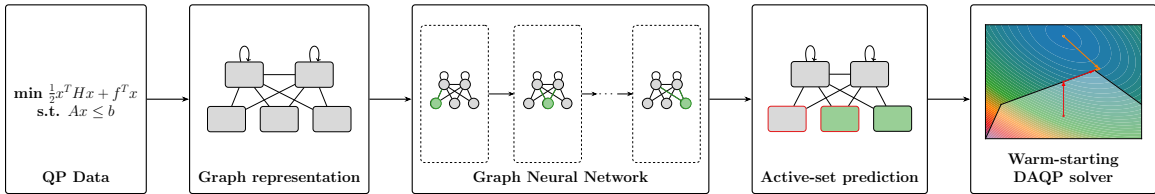


Figure 1: Method overview: The problem is formulated as a QP and represented as a graph, which serves as input to the Graph Neural Network (GNN) for node-level prediction. The resulting prediction is then used to warm-start the DAQP solver.

which are subsequently used to obtain a candidate solution. Prior work has also explored learning penalty parameters for splitting-based QP solvers (Ichnowski et al., 2021), or predicting search directions for interior-point methods using LSTMs (Gao et al., 2024). Further approaches using hybrid methods use classification trees or k-NN classifiers (Klaučo et al., 2019), neural networks (Chen et al., 2022a) or transformers (Zinage et al., 2024) to predict active constraints. However, most machine-learning-based approaches for active-set methods ignore the structural properties inherent in optimization problems (Klaučo et al., 2019; Chen et al., 2022a; Zinage et al., 2024).

In contrast, we investigate how graph neural networks (GNN) accelerate the active-set method for solving QPs. This technique leverages the underlying problem structure using graphs similar to Sjölund and Bänkestad (2022); Häusner et al. (2024, 2025). Instead of computing each iteration precisely, the proposed approach predicts the active set allowing the solver to omit multiple iterations and thereby significantly reduce computation time. The whole method overview is depicted in Figure 1. GNNs are particularly well-suited for this task since they inherently capture the structural properties of QPs. They are invariant to node permutations, corresponding to reordering constraints, and can exploit sparsity patterns effectively (Cappart et al., 2023). Previous work has transformed QPs into graph representations to study whether GNNs can map problems to optimal solutions (Chen et al., 2024). While these studies provide theoretical insights, they lack extensive experimental validation, which we address in this paper.

The main contributions of this paper are therefore (i) designing a GNN-based approach to accelerate QP solving by learning the active set, and (ii) a comprehensive evaluation of the proposed method in terms of scalability to different input sizes.

2. Background

In this paper, we use machine learning to accelerate solving convex quadratic programs (QPs) with linear inequality constraints,

$$\underset{x \in \mathbb{R}^n}{\text{minimize}} \quad \frac{1}{2} x^T H x + f^T x, \quad \text{subject to} \quad Ax \leq b. \quad (1)$$

The objective function is defined by the positive definite matrix $H \in \mathbb{R}^{n \times n}$ and the vector $f \in \mathbb{R}^n$. The feasible solution space is defined by $A \in \mathbb{R}^{m \times n}$ and $b \in \mathbb{R}^m$. Due to convexity the global optimum can be found efficiently, with computational difficulty comparable to that of linear programs (Nocedal and Wright, 1999).

Many applications require solving a sequence of similar QPs, where only specific parameters change between iterations. We consider problems where the parameter $\eta \in \mathbb{R}^p$ only affects the

linear term in the objective function f and the right-hand side of the constraints b , i.e.

$$\underset{x \in \mathbb{R}^n}{\text{minimize}} \quad \frac{1}{2} x^T H x + f(\eta)^T x, \quad \text{subject to} \quad Ax \leq b(\eta). \quad (2)$$

Hence, the overall problem structure is the same across problem instances.

2.1. Active-set method

The active-set method is an iterative solution method for QPs that aims to identify the active set $\mathcal{A}^* \subseteq \{1, 2, \dots, m\}$, consisting of all inequality constraints that hold with equality, at an optimal solution x^* . Knowing the active set simplifies the system by transforming an inequality-constraint problem into one with a reduced set of equality constraints, as stated in Lemma 3.1 in [Arnström \(2023\)](#). The resulting linear system can be solved in a single iteration by matrix factorization techniques.

To identify the active set \mathcal{A}^* , a working set \mathcal{W} serves as an approximation of the active set that is updated iteratively. At each iteration, one constraint is either added to or removed from \mathcal{W} until the active set of an optimal solution x^* is found and the linear system can be solved in a single iteration. Solvers initialized with an empty working set $\mathcal{W}_0 = \emptyset$ are said to be cold-started. In contrast, warm-started solvers begin with a non-empty working set $\mathcal{W}_0 \neq \emptyset$, which can significantly reduce the number of iterations needed to identify the active set and thereby the optimum ([Otta et al., 2015](#); [Arnström, 2023](#)). While the improvement is most pronounced when the working set \mathcal{W}_0 closely matches the true active set, even a partial overlap can reduce the iteration count noticeably. This forgiving aspect motivates a learning-to-optimize approach: making a perfect guess is hard (as it essentially amounts to finding the optimum) but from previous problem instances we hope to come reasonably close, and thereby achieve practically significant acceleration.

2.2. Dual active-set solver

To benefit from warm-starting, we apply the dual active-set solver proposed by [Arnström et al. \(2022\)](#). Unlike primal solvers, which require a feasible initial iterate x_0 , dual solvers are easier to warm-start, as the non-negativity of the dual variables always allows $\lambda_0 = 0$ as a feasible starting point. The DAQP solver¹ follows Algorithm 1 (Appendix A) from [Arnström et al. \(2022\)](#) and leverages an LDL^T factorization for efficient numerical updates. Since the working set changes by at most one constraint per iteration, the lower unit triangular matrix L and diagonal matrix D can be updated via rank-one modifications, reducing computational complexity. Singularity is directly detected from the diagonal of D , and the main computations are performed using forward/backward substitution, avoiding explicit matrix inversion. The extent to which previous computations can be reused depends on the change in the working set \mathcal{W} at each iteration. Specifically, if the modification occurs near the end of the working set, most of the previous factorization can be reused, whereas changes earlier in the set require recomputation of a larger portion during the substitution steps.

2.3. Graph Neural Networks

Graph neural networks (GNN) refer to neural network architectures for operating on graphs. The graphs are defined by the vertex set V and the directed edge set $E \subseteq V \times V$. For each vertex $s \in V$,

1. <https://github.com/darnstrom/daqp>

we assign a vertex feature vector $x_s \in \mathbb{R}^{d_v}$, while each directed edge $e_{ts} \in E$ from vertex t to vertex s is associated with an edge feature vector $z_{ts} \in \mathbb{R}^{d_e}$. The model consists of multiple GNN layers, where each layer updates vertex and edge features. In this paper, we follow the framework of message-passing GNNs in [Battaglia et al. \(2018\)](#). The update is performed by the permutation-invariant aggregation function \bigoplus , which acts on the neighborhood of each vertex, and the learnable functions ϕ and ψ . Most commonly, the graph structure remains unchanged throughout the process.

The update of layer l begins with computing the edges features for the subsequent layer $l + 1$ using the parametrized message function $\phi_{\theta_z^{(l)}}$

$$z_{ts}^{(l+1)} := \phi_{\theta_z^{(l)}} \left(z_{ts}^{(l)}, x_t^{(l)}, x_s^{(l)} \right), \quad (3)$$

where the output is referred to as message. In the next step, all incoming messages to a vertex s are aggregated by applying the aggregation function \bigoplus over the neighborhood $\mathcal{N}_s = \{t \mid (t, s) \in E\}$,

$$m_s^{(l+1)} := \bigoplus_{t \in \mathcal{N}_s} z_{ts}^{(l+1)}. \quad (4)$$

Common choices for \bigoplus include summation, maximization, and averaging. The outcome $m_s^{(l+1)}$ serves as input for the vertex feature update for layer $l + 1$ by the parametrized function $\psi_{\theta_x^{(l)}}$

$$x_s^{(l+1)} := \psi_{\theta_x^{(l)}} \left(x_s^{(l)}, m_s^{(l+1)} \right). \quad (5)$$

The update functions ϕ and ψ are parametrized by learnable parameters θ ([Bronstein et al., 2021](#)). To apply this method to solve QPs, we next describe how they are represented as graphs.

3. Method

The proposed GNN-based approach for solving QPs comprises three key components: the graph representation of the data, the learned mapping, and the final model architecture.

3.1. Graph representation

We represent the underlying QPs as bipartite graphs following [Chen et al. \(2024\)](#).

Definition 1 *The graph representation of a QP is defined by $G = (W \cup C, E_W \cup E_C)$, where*

- *the set $W = \{1, \dots, n\}$ represents the variable nodes. The i -th vertex represents the i -th variable of the QP and the assigned feature vector $x_s \in \mathbb{R}^w$ captures the corresponding component of f as well as the node type.*
- *the set $C = \{n + 1, \dots, m\}$ represents the constraint nodes. The j -th vertex represents the j -th constraint of the QP and the assigned feature vector $x_s \in \mathbb{R}^c$ captures the corresponding component of b as well as the direction of the inequality sign and the node type.*
- *the edges contained in E_W and their feature vectors are given by the adjacency matrix H , which defines the quadratic term in the QP.*
- *the edges contained in E_C and their feature vectors are given by the adjacency matrix A and show the relations between the variable and constraint nodes.*

This is exemplified in Figure 2.

$$\begin{aligned}
\text{minimize}_{x \in \mathbb{R}^n} \quad & \frac{1}{2} (x_1 \ x_2) \underbrace{\begin{pmatrix} 2 & 1 \\ 1 & 2 \end{pmatrix}}_{=H} \begin{pmatrix} x_1 \\ x_2 \end{pmatrix} + \underbrace{\begin{pmatrix} -4 & -8 \end{pmatrix}}_{=f} \begin{pmatrix} x_1 \\ x_2 \end{pmatrix} \\
\text{subject to} \quad & x_1 + x_2 \leq 3 \\
& -x_1 + 2x_2 \leq 0 \\
& \underbrace{-3x_1 + x_2}_{=A} \leq \underbrace{10}_{=b}.
\end{aligned}$$

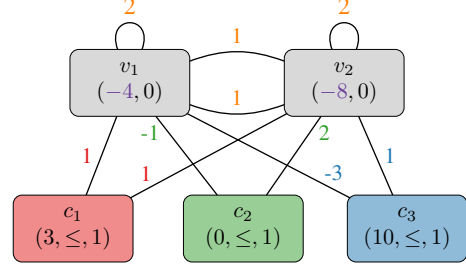


Figure 2: A quadratic program can be represented as a bipartite graph having a set of variable nodes and a set of constraint nodes, with edge features describing relationships between variables.

3.2. Learning problem

The key idea is to learn the parameters θ of a mapping p_θ from a problem instance represented by a graph G to the resulting active set \mathcal{A}^*

$$p_\theta : \mathcal{G} \rightarrow \mathcal{P}(\mathbb{N}_m), \quad p_\theta(G) \approx \mathcal{A}^*, \quad (6)$$

where \mathcal{G} denotes the set of all graphs and \mathcal{P} the power set. This corresponds to a node classification task on the graph G , determining whether each constraint vertex is active or not. Finding this mapping is not trivial, since the optimal solution x^* must be known to determine the active set \mathcal{A}^* (Zinage et al., 2024). The predicted active set is then used to warm-start the solver.

This approach has the potential to automate and improve on the non-trivial task of finding a good initial guess, while retaining the theoretical convergence guarantees of conventional solvers. Moreover, the graph representation implies permutation equivariance, such that the order of constraints does not affect the model. Finally, GNNs can operate on graphs of varying sizes, making them easily adaptable to different QPs (Chen et al., 2024).

3.3. Model architecture

The only restriction our approach places on the GNN architecture is that it can operate on the bipartite graph representation in Definition 1. For the sake of demonstration, this paper uses Local Extrema Convolution (LEConv) layers (Ranjan et al., 2020), we leave the design of tailored layers for this application to future work.

In the LEConv architecture, the edge feature update for layer $l + 1$ is defined by the function $\phi_{\theta_z^{(l)}}$ in Equation (3) as

$$z_{ts}^{(l+1)} := z_{ts}^{(l)} \cdot \left(x_s^{(l)} W_2 - x_t^{(l)} W_3 \right), \quad (7)$$

where $z_{ts}^{(l)}$ represents the feature of the directed edge from node t to s in layer l , $x_s^{(l)}$ and $x_t^{(l)}$ are the corresponding vertex features, and W_j are learnable weight matrices. Sum aggregation as in Equation (4) yields the message for node s in layer $l + 1$

$$m_s^{(l+1)} := \sum_{t \in \mathcal{N}_s} z_{ts}^{(l)} \left(x_s^{(l)} W_2 - x_t^{(l)} W_3 \right). \quad (8)$$

The vertex update function $\psi(\cdot)$, as introduced in Equation (5), then combines the node's previous feature with the aggregated message

$$x_s^{(l+1)} := \sigma \left(x_s^{(l)} W_1 + m_s^{(l+1)} \right) = \sigma \left(x_s^{(l)} W_1 + \sum_{t \in \mathcal{N}_s} z_{ts}^{(l)} \left(x_s^{(l)} W_2 - x_t^{(l)} W_3 \right) \right), \quad (9)$$

where $\sigma(\cdot)$ denotes the activation function.

The final model consists of three layers, an input layer, a hidden layer of width 128 and an output layer. All layers share the same architectural structure, presented above. LeakyRELU was chosen as the activation function with a negative slope of 0.1. A sigmoid activation function is applied to the output layer to interpret the outputs as probabilities of a node being active or not.

The model is trained using the AdamW optimizer with default learning rates and a weighted binary cross-entropy loss, where class weights reflect the empirical class distribution. Early stopping based on validation loss is applied, terminating training if the loss does not improve by at least 0.001 over five consecutive epochs, with the best-performing parameters retained. The threshold for predicting active constraint is set by performing a grid search over $[0, 1]$ with a step size of 0.1.

4. Experiments

The experiments first evaluate the model on synthetic data to assess its ability to predict the active set and compare it against a multilayer perceptron (MLP). Subsequently, the GNN is applied to datasets with varying problem sizes and to an inverted pendulum control problem. The results examine both the predictive accuracy and the impact on solver efficiency. All experiments are conducted on a single NVIDIA Titan Xp GPU.

4.1. Synthetic data generation

Some experiments use synthetic data parameterized by $\eta \in \mathbb{R}^p$ as in Equation (2). To ensure that the matrix in the objective function H is symmetric and positive definite, it is generated using the matrix $M \in \mathbb{R}^{n \times n}$ with $H = MM^T$. If required, sparsity patterns can be applied to both matrices. The right-hand side of the constraints and the linear term in the objective function are defined by affine transformations $f : \mathbb{R}^p \rightarrow \mathbb{R}^n$ and $b : \mathbb{R}^p \rightarrow \mathbb{R}^m$,

$$f(\eta) = \hat{f} + F\eta, \quad b(\eta) = \hat{b} - AT\eta, \quad (10)$$

where $\hat{f} \in \mathbb{R}^n$, $F \in \mathbb{R}^{n \times p}$, $\hat{b} \in \mathbb{R}^m$ and the transformation matrix $T \in \mathbb{R}^{n \times p}$ ensures primal feasibility of $x = T\eta$. All variables are sampled from a standard normal distribution $\mathcal{N}(0, 1)$, with the exception of \hat{b} , which is drawn from a uniform distribution over $[0, 1]$ to ensure that the origin is feasible. This guarantees that the DAQP solver used in the implementation finds a feasible solution.

4.2. Active-set prediction using GNN

To demonstrate the ability of capturing the problem structure using GNNs, an experimental pipeline was implemented following the methods in Section 3. The synthetic data, generated as described in Section 4.1, was converted into graph representations according to Section 3.1 and used as input to the model detailed in Section 3.3.

The evaluation uses standard classification metrics computed only over constraint nodes, as these are the only relevant nodes in this node-level classification task. All metrics are reported as percentages and rounded to two decimal places. As a baseline for comparison, a naïve model that classifies all nodes as inactive, corresponding to cold-starting the solver, is given.

The dataset used contains of 5000 instances with $n = 10$ (variables) and $m = 40$ (constraints). Table 1 shows averages over five different runs with different random seeds. On the test set, the GNN achieves over 89% across all standard metrics, clearly outperforming the naïve baseline (Accuracy 82.96%), indicating its strong predictive capability. The accuracy is the highest metric due to the unbalanced dataset, as each graph contains more inactive than active nodes.

4.3. Impact of problem structure on predictive performance

To assess whether incorporating problem structure through a graph neural network improves predictive performance, we compare it to a standard multilayer perceptron (MLP). For the MLP, all QP components are concatenated into a single input vector by flattening $H \in \mathbb{R}^{n \times n}$ and $A \in \mathbb{R}^{m \times n}$, and appending $f \in \mathbb{R}^n$ and $b \in \mathbb{R}^m$, yielding a vector of size $n^2 + mn + n + m$. The MLP produces binary predictions for all $n + m$ elements, enabling direct comparison with the GNN, though only the m constraint predictions are of primary interest. For each problem size, 2000 QPs are generated, with sparsity introduced via banded matrices M and A . It is important to note, that an MLP has one fixed input size, such that a new model needs to be trained for each different problem size.

The comparison considers the number of iterations (Figure 3) and total solve time (Figure 4) for increasing problem sizes, while maintaining a fixed 1:4 ratio between variable and constraint nodes. All values represent the mean over five independent runs per problem size. Figure 3 shows that cold-starting the DAQP solver requires most iterations, whereas warm-starting with predictions from the machine learning models substantially reduces this count. Iteration growth remains sublinear across all approaches.

Figure 4 compares solve and prediction times for each model type across varying problem sizes. The solve time is measured using the built-in timing functionality of the DAQP solver, combining initialization and computing time, ensuring consistent evaluation conditions. When a model predicts an active set, it is provided as input to the solver. For cold-starting, no such initialization is available, and the problem is solved without prior knowledge. The prediction time refers to the forward pass during testing and all results are averaged over five independent runs. The solve times for all models scale similarly, approximately proportional to $x^{3/2}$ as shown in Appendix B. Even if not clearly visible here, the GNN con-

Metric	Test
Accuracy (%)	95.43 ± 0.4
Precision (%)	89.53 ± 1.4
Recall (%)	89.74 ± 1.7
F1-score (%)	89.62 ± 0.9

Table 1: Metrics of the GNN model trained on synthetic data with $n = 10$ (variables) and $m = 40$ (constraints).

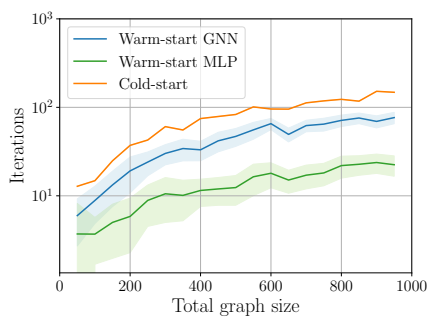


Figure 3: Comparison of iterations when warm-starting the DAQP solver with predictions from our graph neural network, a standard multilayer perceptron and cold-starting the solver without any learned prediction.

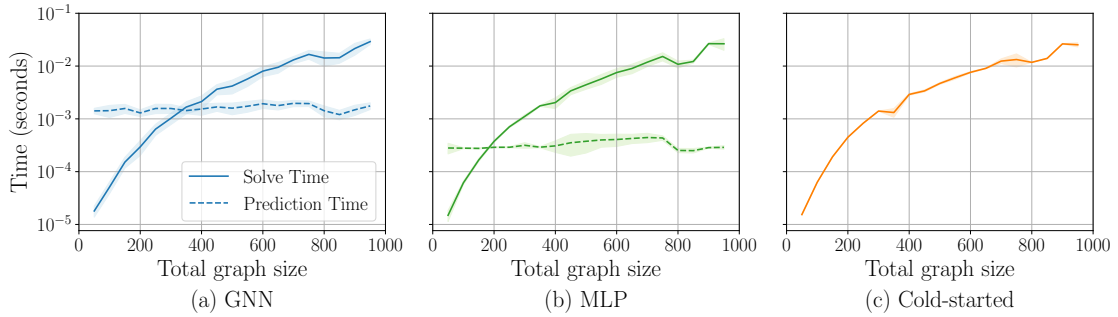


Figure 4: Comparison of solve time and prediction time for (a) our graph neural network, (b) a standard multilayer perceptron, and (c) the cold-started active set method.

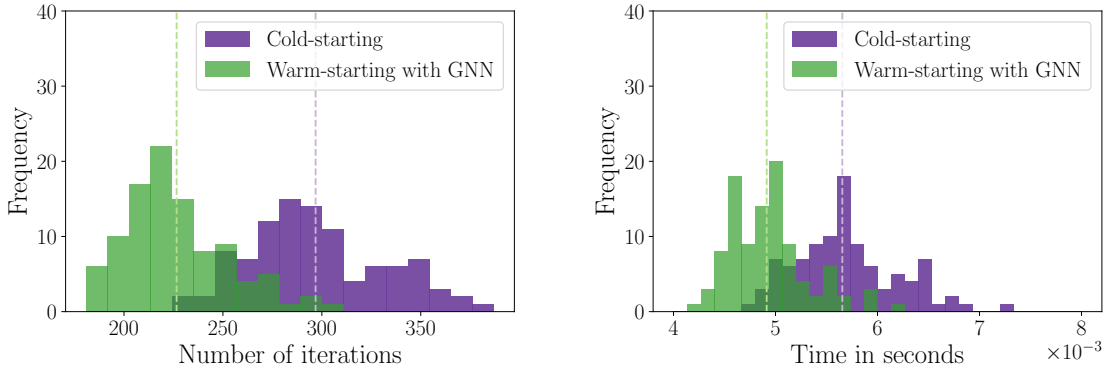


Figure 5: Comparison of iterations (left) and solve time (right) of cold-starting (purple) and warm-starting the DAQP solver using the GNN (green) on problem instances with 100 variables and 200 constraints. The dashed line represents the mean.

sistently reduces solve time compared to cold-starting, as further illustrated in the next section. Both the GNN and MLP exhibit approximately constant prediction times as the problem size increases, with the MLP achieving predictions nearly an order of magnitude faster than the GNN due to its simpler architecture and hardware-optimized implementation.

4.4. Generalization across variable problem sizes

Although the solve time for the GNN and MLP is comparable, and the MLP achieves a slightly lower iteration count, its fixed input size limits its applicability to varying problem sizes. In contrast, GNNs naturally handle graphs of arbitrary size, making them well-suited for scenarios where the number of variables and constraints varies across instances. This flexibility enables generalization across heterogeneous problem structures, offering clear practical advantages.

To illustrate this, the GNN was trained on graphs of size $[60, 120, 180]$ and tested on graphs of size 300. As Figure 5 shows, the model still achieves substantial reductions in iterations and solve time, demonstrating that models trained on smaller problem sizes can generalize effectively to larger ones, reducing the need for retraining and providing practical efficiency gains.

4.5. Effect of predictive model on solver efficiency

To evaluate the impact of the GNN’s predictions on solver performance under realistic conditions, we apply it to the control problem of an inverted pendulum on a cart, generated using the `lmpc` package². The package produces data for model predictive control (MPC) of linear systems, resulting in problems of the form

$$\begin{aligned}
 \underset{u_0, \dots, u_{N_c-1}}{\text{minimize}} \quad & \frac{1}{2} \sum_{k=0}^{N_p-1} ((Cz_k - r)^T Q (Cz_k - r) + u_k^T R u_k + \Delta u_k^T R_r \Delta u_k) \\
 \text{subject to} \quad & z_{k+1} = F z_k + G u_k, \quad k = 0, \dots, N_p - 1 \\
 & z_0 = \hat{z} \\
 & \underline{b} \leq A_z z_k + A_u u_k \leq \bar{b}, \quad k = 0, \dots, N_p - 1,
 \end{aligned} \tag{11}$$

where z_k and u_k are the system state and control action, respectively, at time step k . The current state \hat{z} and a set point r make this a parametric optimization problem. This problem can be condensed (see, for example, Chapter 2 in (Arnström, 2023)) to yield QPs of the form (1), where the decision variable x contains the control actions u_0, \dots, u_{N_c-1} , and the linear term f in the objective function and the right-hand side b of the constraints are affine functions of \hat{z} and r .

Specifically for the inverted pendulum, the control u is a force applied to the cart, and the state is $z = (p, \dot{p}, \phi, \dot{\phi})$, where p is the position of the cart and ϕ is the angle of the pendulum. We have the actuation constraint $|u| \leq 1$ and the state constraints $|p| \leq 10$ and $|\phi| \leq \frac{\pi}{4}$. The specific input parameters used in this implementation can be found in the repository³.

Two datasets with different control horizons are compared, both use a prediction horizon of $N_p = 50$. The first dataset has a the control horizon is set to $N_c = 5$, resulting in 206 input and state constraints, while the second uses $N_c = 50$ with $m = 296$ constraints. The GNN is trained on the generated data, and the results are averaged over five independent runs. A regularization term is added to encourage sparsity in the predicted active sets.

Figure 6 shows both the change in solver iterations and solve time. Warm-starting the QP with the active set predicted by the GNN reduces the number of iterations, with an average reduction of 1.0 iterations on the first dataset and 1.6 iterations on the second one. Table 2 shows that for the dataset with control horizon $N_c = 50$ this reduction is most pronounced for problems that require many iterations in the cold-start scenario, whereas for problems that converge quickly, the benefit is minimal. These iteration savings translate into a corresponding decrease in solving time, consistent with earlier experiments.

Future work could explore a two-step approach: first predicting the number of active constraints, then warm-starting only the problems with many active constraints. This targets cases where warm-starting yields substantial gains, while avoiding unnecessary risk when few iterations are needed.

Percentiles	10%	25%	50 %	75%	90%
Iterations cold-start	3	4	13	55.5	94
Iterations warm-start	3	4	19	47.6	78.7

Table 2: Iteration reduction on dataset with $N_c = 50$.

2. <https://github.com/darnstrom/lmpc>
3. https://github.com/ellaschmidtobreick/acc_daqp

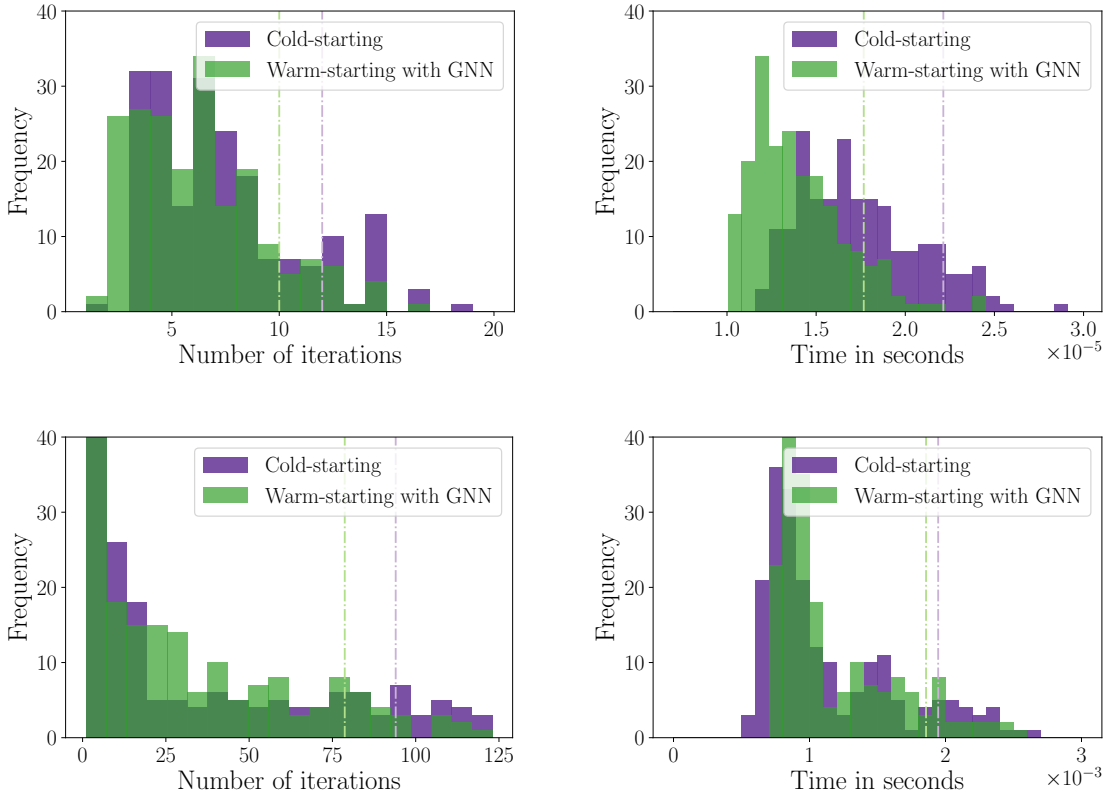


Figure 6: Comparison of iterations (left) and solve time (right) of cold-starting (purple) and warm-starting the DAQP solver using the GNN (green) on problem instances with control horizon 5 (upper row) and 50 (lower row). The prediction horizon is 50 in both cases and the constraints are 206 and 296 respectively. The dash-dotted line refers to the 90% percentile.

5. Conclusion

This work presented a learning-to-optimize approach using graph neural networks to predict the active set in dual active-set solvers for quadratic programs. By representing QPs as bipartite graphs, the model effectively captures their structural properties and enables efficient warm-starting. The experiments demonstrate consistent reductions in solver iterations and solve time, with the largest gains for problems requiring many iterations when cold-started. The approach scales well with increasing problem sizes and generalizes effectively to larger graphs even when only trained on smaller instances, highlighting its flexibility and practical applicability. These results indicate that incorporating learned structure-aware predictions can significantly accelerate optimization in sequential or real-time settings. Future work could extend this approach to other problem classes and further investigate models trained on smaller instances that generalize to larger graphs, reducing training cost. Furthermore, a multi-step approach, first predicting the number of active constraints and then identifying which constraints are active, could improve prediction accuracy and enable faster and more adaptive control in real-world systems.

Acknowledgments

This work was funded by the Swedish Research Council, grant number 2024-04130, and supported by the Wallenberg AI, Autonomous Systems and Software Program (WASP) funded by the Knut and Alice Wallenberg Foundation. The computations were enabled by resources provided by the National Academic Infrastructure for Supercomputing in Sweden (NAIIS), partially funded by the Swedish Research Council through grant agreement no. 2022-06725.

References

Brandon Amos. Tutorial on amortized optimization. *Foundations and Trends® in Machine Learning*, 16(5):592–732, 2023.

Marcin Andrychowicz, Misha Denil, Sergio Gómez, Matthew W Hoffman, David Pfau, Tom Schaul, Brendan Shillingford, and Nando de Freitas. Learning to learn by gradient descent by gradient descent. In *Advances in Neural Information Processing Systems*, volume 29. Curran Associates, Inc., 2016.

Daniel Arnström. *Real-Time Certified MPC : Reliable Active-Set QP Solvers*. PhD thesis, Linköping University, 2023.

Daniel Arnström, Alberto Bemporad, and Daniel Axehill. A Dual Active-Set Solver for Embedded Quadratic Programming Using Recursive LDL^t Updates. *IEEE Transactions on Automatic Control*, 67(8):4362–4369, 2022.

Sebastian Banert, Jevgenija Rudzusika, Ozan Öktem, and Jonas Adler. Accelerated forward-backward optimization using deep learning. *SIAM Journal on Optimization*, 34(2):1236–1263, 2024.

Roscoe A. Bartlett, Lorenz T. Biegler, Johan Backstrom, and Vipin Gopal. Quadratic programming algorithms for large-scale model predictive control. *Journal of Process Control*, 12(7):775–795, 2002.

Peter W. Battaglia, Jessica B. Hamrick, Victor Bapst, Alvaro Sanchez-Gonzalez, Vinicius Zambaldi, Mateusz Malinowski, Andrea Tacchetti, David Raposo, Adam Santoro, Ryan Faulkner, Caglar Gulcehre, Francis Song, Andrew Ballard, Justin Gilmer, George Dahl, Ashish Vaswani, Kelsey Allen, Charles Nash, Victoria Langston, Chris Dyer, Nicolas Heess, Daan Wierstra, Pushmeet Kohli, Matt Botvinick, Oriol Vinyals, Yujia Li, and Razvan Pascanu. Relational inductive biases, deep learning, and graph networks, 2018. arXiv:1806.01261.

Francesco Borrelli, Alberto Bemporad, and Manfred Morari. *Predictive control for linear and hybrid systems*. Cambridge University Press, 2017.

Michael M. Bronstein, Joan Bruna, Taco Cohen, and Petar Veličković. Geometric Deep Learning: Grids, Groups, Graphs, Geodesics, and Gauges, 2021. arXiv:2104.13478.

Quentin Cappart, Didier Chételat, Elias B. Khalil, Andrea Lodi, Christopher Morris, and Petar Veličković. Combinatorial Optimization and Reasoning with Graph Neural Networks. *Journal of Machine Learning Research*, 24(130):1–61, 2023.

Steven W. Chen, Tianyu Wang, Nikolay Atanasov, Vijay Kumar, and Manfred Morari. Large scale model predictive control with neural networks and primal active sets. *Automatica*, 135:109947, 2022a.

Tianlong Chen, Xiaohan Chen, Wuyang Chen, Howard Heaton, Jialin Liu, Zhangyang Wang, and Wotao Yin. Learning to optimize: A primer and a benchmark. *Journal of Machine Learning Research*, 23(189):1–59, 2022b.

Ziang Chen, Xiaohan Chen, Jialin Liu, Xinshang Wang, and Wotao Yin. Expressive Power of Graph Neural Networks for (Mixed-Integer) Quadratic Programs, 2024. arXiv:2406.05938.

Henri Doerks, Paul Häusner, Daniel Hernández Escobar, and Jens Sjölund. Learning to accelerate distributed ADMM using graph neural networks. *arXiv preprint arXiv:2509.05288*, 2025.

Xi Gao, Jinxin Xiong, Akang Wang, Qihong Duan, Jiang Xue, and Qingjiang Shi. IPM-LSTM: A learning-based interior point method for solving nonlinear programs. *Advances in Neural Information Processing Systems*, 37:122891–122916, 2024.

Jacek Gondzio and Andreas Grothey. Parallel interior-point solver for structured quadratic programs: Application to financial planning problems. *Ann Oper Res*, 152(1):319–339, 2007.

Martin Herceg, CN Jones, and M Morari. Dominant speed factors of active set methods for fast MPC. *Optimal Control Applications and Methods*, 36(5):608–627, 2015.

Paul Häusner, Ozan Öktem, and Jens Sjölund. Neural incomplete factorization: learning preconditioners for the conjugate gradient method. *Transactions on Machine Learning Research*, 2024.

Paul Häusner, Aleix Nieto Juscafresa, and Jens Sjölund. Learning incomplete factorization preconditioners for GMRES. In *Proceedings of the 6th Northern Lights Deep Learning Conference (NLDL)*, pages 85–99. PMLR, 2025.

Jeffrey Ichnowski, Paras Jain, Bartolomeo Stellato, Goran Banjac, Michael Luo, Francesco Borrelli, Joseph E Gonzalez, Ion Stoica, and Ken Goldberg. Accelerating Quadratic Optimization with Reinforcement Learning. In *Advances in Neural Information Processing Systems*, volume 34, pages 21043–21055. Curran Associates, Inc., 2021.

Martin Klaučo, Martin Kalúz, and Michal Kvasnica. Machine learning-based warm starting of active set methods in embedded model predictive control. *Engineering Applications of Artificial Intelligence*, 77:1–8, 2019.

Scott Kuindersma, Frank Permenter, and Russ Tedrake. An efficiently solvable quadratic program for stabilizing dynamic locomotion. In *2014 IEEE International Conference on Robotics and Automation (ICRA)*, pages 2589–2594, 2014.

Gautam Mitra, Frank Ellison, and Alan Scowcroft. Quadratic programming for portfolio planning: Insights into algorithmic and computational issues. *J Asset Manag*, 8(3):200–214, 2007.

Jorge Nocedal and Stephen J. Wright, editors. *Numerical Optimization*. Springer Series in Operations Research and Financial Engineering. Springer-Verlag, New York, 1999.

Pavel Otta, Ondrej Santin, and Vladimir Havlena. Measured-state driven warm-start strategy for linear MPC. In *2015 European Control Conference (ECC)*, pages 3132–3136, 2015.

Ekagra Ranjan, Soumya Sanyal, and Partha Pratim Talukdar. ASAP: Adaptive Structure Aware Pooling for Learning Hierarchical Graph Representations, 2020. arXiv:1911.07979.

Rajiv Sambharya and Bartolomeo Stellato. Learning algorithm hyperparameters for fast parametric convex optimization. *arXiv preprint arXiv:2411.15717*, 2024.

Rajiv Sambharya, Georgina Hall, Brandon Amos, and Bartolomeo Stellato. End-to-End Learning to Warm-Start for Real-Time Quadratic Optimization. In *Proceedings of The 5th Annual Learning for Dynamics and Control Conference*, pages 220–234. PMLR, 2023.

Jens Sjölund and Maria Båkestad. Graph-based Neural Acceleration for Nonnegative Matrix Factorization, 2022. arXiv:2202.00264.

Vrushabh Zinage, Ahmed Khalil, and Efstathios Bakolas. TransformerMPC: Accelerating Model Predictive Control via Transformers, 2024. arXiv:2409.09266.

Appendix A. Algorithm of the DAQP solver

Algorithm 1 Dual active-set method for solving a dual QP (Arnström et al., 2022)

Require: $M, d, v, R^{-1}, \mathcal{W}_0, \lambda_0$

Ensure: $x^*, \lambda^*, \mathcal{A}^*$

```

1: while true do
2:   if  $M_{\mathcal{W}}M_{\mathcal{W}}^T$  is nonsingular then
3:     Solve  $M_{\mathcal{W}}M_{\mathcal{W}}^T\lambda_{\mathcal{W}}^* = -d_{\mathcal{W}}$ 
4:     if  $\lambda^* \geq 0$  then
5:        $\mu_{\mathcal{W}} \leftarrow M_{\mathcal{W}}M_{\mathcal{W}}^T\lambda_{\mathcal{W}}^* + d_{\mathcal{W}}$ 
6:        $\lambda \leftarrow \lambda^*$                                      //  $\lambda^*$  dual feasible
7:       if  $\mu \geq 0$  then
8:         break                                              //  $x^*$  primal feasible
9:       else
10:       $j \leftarrow \arg \min_{i \in \mathcal{W}} [\mu]_i$            //  $x^*$  not primal feasible
11:       $\mathcal{W} \leftarrow \mathcal{W} \cup \{j\}$ 
12:    end if
13:  else
14:     $p \leftarrow \lambda^* - \lambda$                            //  $\lambda^*$  not dual feasible
15:     $\mathcal{B} \leftarrow \{i \in \mathcal{W} \mid [\lambda^*]_i < 0\}$ 
16:     $(\lambda, \mathcal{W}) \leftarrow \text{FIXCOMPONENT}(\lambda, \mathcal{W}, \mathcal{B}, p)$ 
17:  end if
18:  else
19:    Solve  $M_{\mathcal{W}}M_{\mathcal{W}}^Tp_{\mathcal{W}} = 0$ 
20:     $\mathcal{B} \leftarrow \{i \in \mathcal{W} \mid [p]_i < 0\}$ 
21:     $(\lambda, \mathcal{W}) \leftarrow \text{FIXCOMPONENT}(\lambda, \mathcal{W}, \mathcal{B}, p)$ 
22:  end if
23: end while
24:  $x^* \leftarrow -R^{-1}(M_{\mathcal{W}}^T\lambda_{\mathcal{W}}^* + v)$ 
25: return  $(x^*, \lambda^*, \mathcal{W})$ 

```

26: **procedure** FIXCOMPONENT($\lambda, \mathcal{W}, \mathcal{B}, p$)

```

27:    $j \leftarrow \arg \min_{i \in \mathcal{B}} \left( -\frac{[\lambda]_i}{[p]_i} \right)$ 
28:    $\mathcal{W} \leftarrow \mathcal{W} \setminus \{j\}$ 
29:    $\lambda \leftarrow \lambda - \frac{[\lambda]_j}{[p]_j} p$ 
30: return  $(\lambda, \mathcal{W})$ 

```

Appendix B. Scaling results on log-log axes

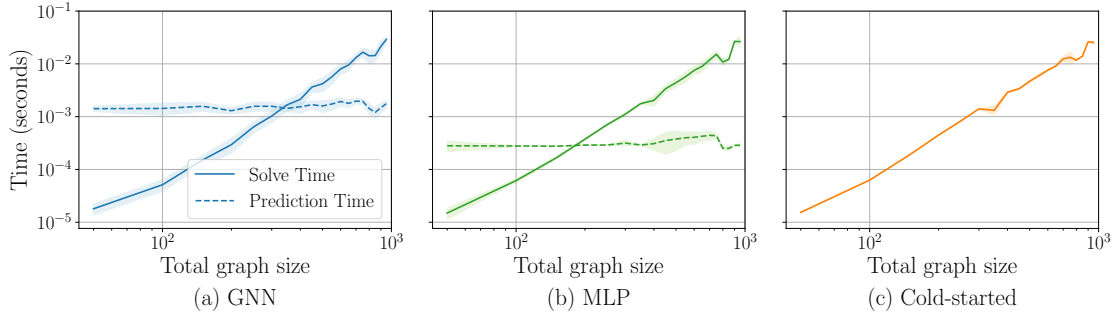


Figure 7: Comparison of solve time (red) and prediction time (purple) for our graph neural network (a), a standard multilayer perceptron (b), and the cold-started active set method (c), shown on logarithmic axes. For the largest graph sizes, the solve time with GNN warm-starting is about five times shorter than the other two, with a negligible prediction time.

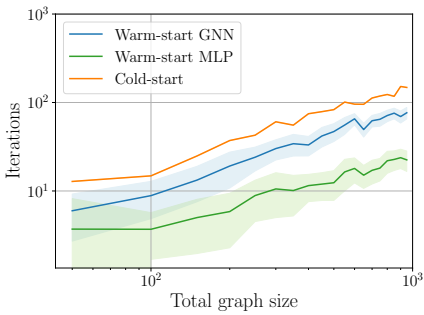


Figure 8: Comparison of iterations when warm-starting the DAQP solver with predictions from our graph neural network, a standard multilayer perceptron and cold-starting the solver without any learned prediction, shown on logarithmic axes.